

Density effect on relativistic electron beams in a plasma fiber

C. T. Zhou,^{1,2,3,a)} X. G. Wang,³ S. Z. Wu,¹ H. B. Cai,^{1,2} F. Wang,² and X. T. He^{1,2,3}

¹Institute of Applied Physics and Computational Mathematics, Beijing 100094, People's Republic of China

²Center for Applied Physics and Technology, Peking University, Beijing 100871, People's Republic of China

³Institute for Fusion Theory and Simulation, Zhejiang University, Hangzhou 310027, People's Republic of China

(Received 23 September 2010; accepted 2 November 2010; published online 18 November 2010)

Intense short-petawatt-laser driven relativistic electron beams in a hollow high- Z plasma fiber embedded in low- Z plasmas of different densities are studied. When the plasma is of lower density than the hollow fiber, resistive filamentation of the electron beam is observed. It is found that the electron motion and the magnetic field are highly correlated with tens of terahertz oscillation frequency. Depending on the material property around the hollow fiber and the plasma density, the beam electrons can be focused or defocused as it propagates in the plasma. Relativistic electron transport and target heating are also investigated. © 2010 American Institute of Physics.

[doi:10.1063/1.3518720]

Recently, lasers with intensities of two orders of magnitude beyond today's state of the art have been planned in the foreseeable future.^{1,2} Such lasers allow important research and application of relativistic plasma physics issues,^{3–12} ranging from compact particle and light sources, fast ignition in inertial confinement fusion, high energy density physics, etc. When a laser pulse interacts with a foil target, electrons produced at the relativistic critical density can be accelerated to relativistic energy by the ponderomotive force.¹³ Nonlinear interaction between these beam electrons and the overdense plasma can lead to changes in the angular characteristics of the beam and nonuniform heating of the cold background plasma. Experiments and simulations^{7,14} show that beam divergence can become large when laser intensity increases. To control the transverse divergence of the beam propagating in the target, several schemes for improving the beam collimation have been proposed recently. These include the use of special target configurations^{6,12} such as the cone-wire, the cone-funnel, the cone-hollow, and the vacuum gap targets. In the plasma-vacuum interface based approaches,^{6,7,15} the guiding of electrons by large surface electric fields generated around the target surface enables the electrons to propagate a long distance at a diameter similar to that of the plasma target. However, when the target is attached to a plasma, the interface is not plasma-vacuum, and recent studies^{16,17} have shown that robust tens of megagauss interface magnetic fields are generated because of the resistivity and density gradients at the material interface. Such magnetic fields can considerably reduce the divergence of the electron beam. Although magnetic-field collimation has been intensively investigated,^{6,7,16,17} it is not clear if these results remain valid for the hollow-guided scheme. In this Letter, we investigate the electron-beam transport and plasma heating when laser-driven relativistic electrons propagate in a hollow fiber immersed in a plasma. In particular, we are interested in the microturbulence behavior of the relativistic electrons.

As shown in Fig. 1(a), we consider that a hollow high- Z gold plasma fiber is attached to a thin disk (slab). The fiber is

embedded in the low- Z plasma (here the deuterium-tritium plasma with $Z=1$ is considered). The two-dimensional model of the target structure is shown in Fig. 1. Both the slab and the hollow consist of gold plasma with a constant degree of ionization $Z=20$. To see how the hollow fiber controls and guides the relativistic electrons, we present the propagation dynamics of the injected electron beam for three cases. In case I, only the slab-hollow target is present. In cases II and III, the hollow is completely embedded in the uniform low- Z plasma. The densities of the low- Z plasma are $n_{\text{low-Z}} = n_{\text{Au}}/10$ and $10n_{\text{Au}}$, respectively, for the cases II and III, as shown in Figs. 3(d) and 3(g) by the thick green solid lines. We simulate the subsequent beam-plasma interaction by directly injecting a high-current electron beam from the left and follow its propagation and evolution. The beam is assumed to have a relativistic-Maxwellian distribution with an average temperature of 1.5 MeV along the x direction. Its width at $1/e^2$ maximum is $20 \mu\text{m}$ and its angular spread is 30° at $(z,x)=(20,0) [\mu\text{m}]$. The beam rises to its maximum value in 50 fs and remains constant at 10^{13} A/cm^2 . The simulation box (z,x) is $200 \mu\text{m} \times 100 \mu\text{m}$. In the present hybrid simulation,¹⁶ the background plasma electrons and ions are treated as fluids and the injected beam electrons are treated by particle-in-cell simulation.

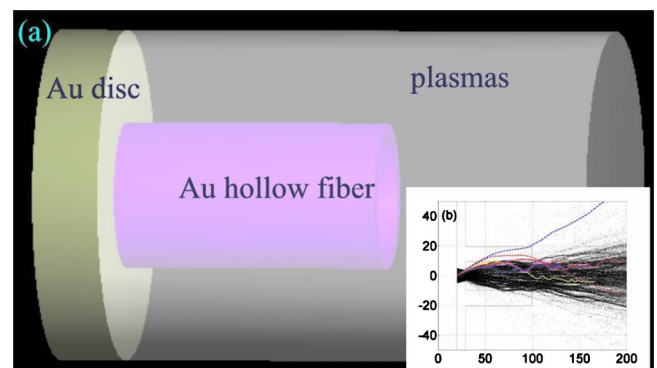


FIG. 1. (Color online) (a) Schematic of the gold-hollow plasma fiber around the low-density deuterium-tritium plasma. (b) The behavior of the beam electrons at $t=1$ ps. The thin dashed lines in (b) show the edges of the gold plasma. The trajectories of several typical electrons initially at $(x,z)=(0,20)$ show the propagation of the beam electrons in the plasma.

^{a)}Electronic mail: zcangtao@iapcm.ac.cn.

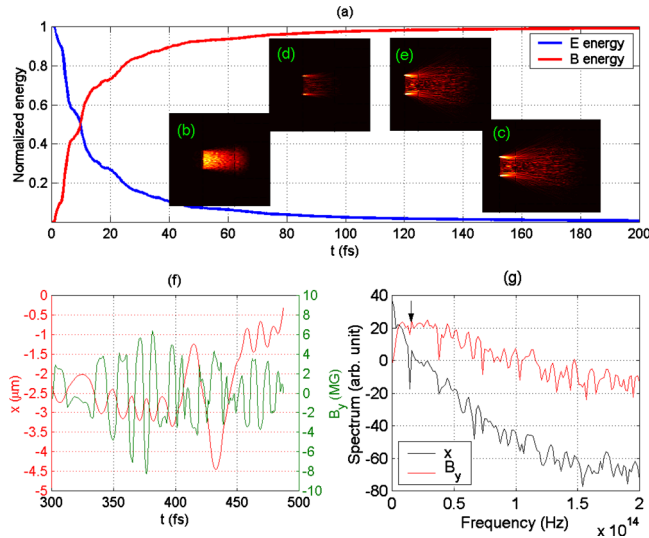


FIG. 2. (Color online) (a) Normalized energy of the electric and magnetic fields. The insets (b) and (c) show the electric field at $t=50$ and 200 fs, respectively. The insets (d) and (e) show the corresponding magnetic fields. (f) Evolution of the trajectory $x(t)$ of a typical beam electron and the magnetic field $B_y(t)$ around it and (g) the corresponding power spectra.

We first consider the relativistic electron transport for case II, as shown in Fig. 1. Initially, the relativistic electron propagation in the gold plasmas will set up a charge separation field, whose energy is then converted into the thermal energy of the plasma by Joule heating. The resistivity as well as the space-charge field is thus reduced, allowing the energetic electrons to propagate further into the plasmas. Since the beam current far exceeds the Alfvén current, the beam transport is possible only if sufficient current neutralization is effected by a return current of background plasma electrons. In the initial stage, the electron currents are in near equilibrium with each other and no resistive magnetic field is generated. As the electron beams propagate further into the target, nonuniform electric fields [see Figs. 2(b) and 2(c)] are induced. The latter can give rise to a magnetic field B_y [see Figs. 2(d) and 2(e)]. This stage leads to an exponential reduction of the electric field and growth of the magnetic field, as shown in Fig. 2(a). When the magnetic energy further increases, the B_y component of the magnetic field can reach several tens of megagauss and is strong enough to pinch the beam electrons. It finally saturates due to magnetic trapping of the beam electrons. The physical processes of exponential reduction of the electric field and growth of the magnetic field can be clearly observed in Figs. 2(a)–2(e).

When the electron beam further enters the gold slab, a strong edge magnetic field, as shown in Figs. 2(d) and 2(e), is generated by $\eta \nabla \times \mathbf{j}_f$, where \mathbf{j}_f and η are the fast electron current and the Spitzer resistivity, respectively. This pushes the beam electrons toward the regions of higher current density and focuses the beam. The beam electrons deposit their energy to the background plasma through the return current. Joule heating of the cold background plasma in the return current [Fig. 3(f)] can be described by the cold-electron energy equation $\partial T_e / \partial t \approx 2J_e^2 / 3\sigma n_e$, where σ and J_e are the electrical conductivity and the cold-electron current density, respectively. Since the resistivity decreases as the plasma is heated by the hot electrons, the resistivity gradient can appear at the beam-plasma edge. The source term $\nabla \eta \times \mathbf{j}_f$ therefore generates a magnetic field when there is a beam

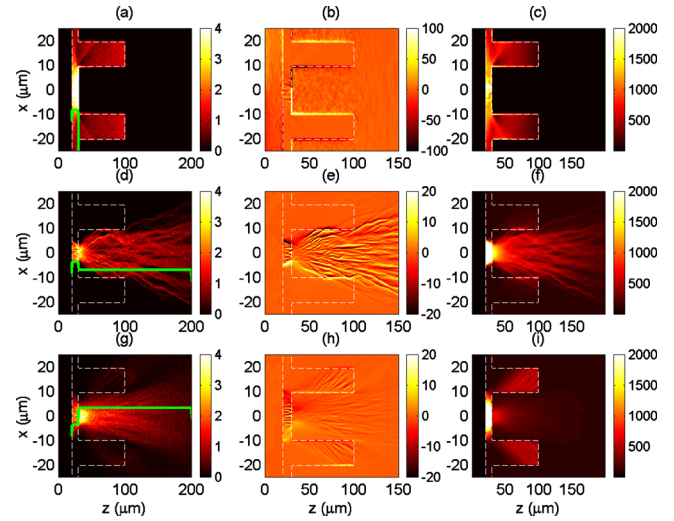


FIG. 3. (Color online) The beam-electron density (n_b/n_{cr}), the magnetic field B_y (in megagauss), and the plasma electron temperature (in eV) at $t=1$ ps. The thin dashed lines in the subplots show the gold plasma and the thick solid lines in (a), (d), and (g) mark the electron density profile of the gold slab and the deuterium-tritium plasma in the beam propagation direction. The first, second, and third rows correspond to cases I, II, and III, respectively.

current perpendicular to a resistivity gradient. For a uniform plasma, this edge magnetic field hollows rather than focuses the beam. The unbalance between the focusing and the defocusing results in complex dynamics of the beam propagation. Figures 1(b) and 3(d) clearly indicate hosing-like instabilities of the beam in the overdense plasma. On the other hand, when the beam electrons propagate in the relatively low-density low- Z plasma, the high-current beam is also subject to a wide range of instabilities, such as the two-stream, Weibel, and filamentation instabilities. The two-stream instability results in the generation of Langmuir turbulence. The Weibel instability leads to the break up of the fast electron beam into small beamlets with a typical transverse dimension of the order of the collisionless skin depth or the Bennett radius¹⁸ $\sqrt{8}(c/v)\lambda_b$, where v is the propagation velocity and λ_b is the Debye length of the electron beam obtained from the transverse temperature. Figure 1(b) exhibits a high degree of filamentation. The beamlets can also coalesce on a longer time scale. These collective effects can result in changes in the angular characteristics of the filamentation beam.

We now investigate how the microturbulent self-generated magnetic field affects the beam electron transport dynamics in the low- Z plasma. The resistive filamentation instability associated with the magnetic field is clearly observed in Figs. 3(d) and 3(e). In order to analyze the microturbulent dynamics of the beam electrons and the magnetic fields, we trace the trajectory $x(t)$ of one of the beam electrons, as shown in Fig. 1(b), and compare it with the magnetic field $B_y(t)$ around it, as shown in Fig. 2(f). We see that the magnetic field can reach several megagauss, which is strong enough to change the propagation direction of the beam electron. The electron motion and the magnetic field are highly correlated. The power spectra of $x(t)$ and $B_y(t)$ are given in Fig. 2(g), which shows a typical chaotic behavior. As indicated by the arrow in Fig. 2(g), $x(t)$ and $B_y(t)$ have the same fundamental frequency, $f_0 \approx 16$ THz. This can correspond to very short period (therefore very short wave-

length or spatial scale) plasma wave oscillations.

In order to have a better understanding of the beam electrons propagating in different density plasmas, we now compare their transport dynamics and heating for the three cases. Figure 3 summarizes the simulation results. For case I, the beam electrons first traverse the plasma slab and exit into the rear vacuum region, and generate large space-charge electrostatic fields at the front and back sides of the slab. These fields create across the plasma slab an electrostatic potential wall and result in multiple reflections of some beam electrons in the slab. By following the electron trajectories, we find that most beam electrons can propagate through the slab to the hollow fiber. A strong azimuthal surface magnetic field ($B_y \sim 100$ MG) [see Fig. 3(b)] and a strong transverse electric field ($E_x \sim 10^{12}$ V/m) surrounding the fiber plasma are created. The surface electric and magnetic fields in the inner and outer surfaces of the fiber confine and guide the hot electrons. The appearance of the thin enhanced return-current layers in both the inner and outer surfaces of the fiber plasma results in enhanced surface heating. The temperature in both surfaces can double that of the bulk of the fiber plasma, as shown in Fig. 3(c).

For cases II and III, the hollow gold plasma fiber is completely embedded in the deuterium-tritium plasma. The interface electric field (several times 10^9 V/m) of the gold slab and the plasma is not strong enough to stop the high-energy electrons. These beam electrons can propagate into the plasma, but their dynamic behaviors are quite different in cases II and III. The interface magnetic field between the gold fiber and the low-Z plasma is mainly from the density and resistivity gradients, etc. The steepest gradients of both at the interface discontinuity (between the different layers) lead to the largest interface magnetic fields. If we assume the Spitzer resistivity $\eta = 10^{-4} Z \ln \Lambda T^{-3/2}$, we can describe the interface magnetic field growth by $\partial \mathbf{B} / \partial t \sim \nabla \eta \times \mathbf{j}_f \sim T_{\text{low-Z}}^{3/2} - T_{\text{high-Z}}^{3/2}$. For case II, it can be seen from Fig. 3(f) that $T_{\text{low-Z}} > T_{\text{high-Z}}$ on both sides of the fiber's inner surface. Thus, on the inner surface, we have $B_y|_{x=10} < 0$ because the sign of \mathbf{j}_f is negative. This interface magnetic field [> 20 MG, shown in Fig. 3(e)] can significantly change the direction of the beam because of the $\mathbf{j} \times \mathbf{B}$ force. Figures 1(b) and 3(d) show that the collimating magnetic field focuses the beam electrons propagation into the deuterium-tritium plasmas inside the fiber. For case III, however, the inner surface magnetic field becomes $B_y|_{x=10} > 0$ because $T_{\text{low-Z}} < T_{\text{high-Z}}$. It is seen from Figs. 3(g) and 3(h) that the beam electrons can be attracted into the gold fiber. When the beam electrons further propagate into the high-density deuterium-tritium plasma, they can also be scattered into the gold fiber through collisions with the background electrons and ions. The enhanced magnetic potential around the fiber then bends the beam electrons such that they propagate along the gold fiber. Higher heating in the gold fiber than in the deuterium-tritium plasma is clearly observed in Fig. 3(i).

In summary, using two-dimensional hybrid simulation, we have investigated the microturbulent dynamics of relativistic electrons driven by petawatt-picosecond pulse lasers in a hollow-guided high-Z gold plasma fiber. We compared the transport and heating of the relativistic electrons propagating in a hollow fiber filled with low-Z deuterium-tritium plasmas

of different densities. It is shown that with a hollow-vacuum target, the surface electric and magnetic fields in the inner and outer surfaces of the fiber confine and guide the hot electrons. The appearance of thin enhanced return-current layers in both the inner and outer surfaces of the fiber plasma results in enhanced surface heating. When the hollow is filled with different density plasmas, a different nonlinear behavior of the electron beam is observed. When the low-Z deuterium-tritium plasma has a lower density than the gold hollow fiber, the inner surface magnetic field due to the steep gradients of the resistivity and plasma density at the interface discontinuity behaves like a plasma mirror, and the resulting reflections of the electron trajectories control the beam electrons in the low-Z plasma. Our simulation results also indicate that the beam electrons and the self-generated microturbulent magnetic field are strongly correlated. However, when the low-Z deuterium-tritium plasma has higher density than the gold hollow fiber, the interface magnetic field in the inner surface of the hollow can change sign so that the relativistic electrons are attracted into the hollow fiber. The findings here may be useful in the design of fast-ignition targets and more efficient point light sources, as well as in other applications of intense laser-driven relativistic electrons.

This work is supported by the National Natural Science Foundation of China (Grant Nos. 10974022 and 10835003) and the National Basic Research Program of China (Grant No. 2007CB815101).

- ¹V. Yanovsky, V. Chvykov, G. Kalinchenko, P. Rousseau, T. Planchon, T. Matsuoka, A. Maksimchuk, J. Nees, G. Cheriaux, G. Mourou, and K. Krushelnick, *Opt. Express* **16**, 2109 (2008).
- ²T. Feder, *Phys. Today* **63**(6), 20 (2010).
- ³J. Zhang, E. E. Fill, Y. Li, D. Schlögl, J. Steingruber, M. Holden, G. J. Tallents, A. Demir, P. Zeitoun, C. Danson, P. A. Norreys, F. Walsh, M. H. Key, C. L. Lewis, and A. G. McPhee, *Opt. Lett.* **21**, 1035 (1996).
- ⁴J. Meyer-ter-Vehn, *Plasma Phys. Controlled Fusion* **51**, 124001 (2009).
- ⁵H. Hora, B. Malekynia, M. Ghoranneviss, G. H. Miley, and X. He, *Appl. Phys. Lett.* **93**, 011101 (2008).
- ⁶C. T. Zhou, L. Y. Chew, and X. T. He, *Appl. Phys. Lett.* **97**, 051502 (2010), and references therein.
- ⁷J. S. Green, K. L. Lancaster, K. U. Akli, C. D. Gregory, F. N. Beg, S. N. Chen, D. Clark, R. R. Freeman, S. Hawkes, C. Hernandez-Gomez, H. Habara, R. Heathcote, D. S. Hey, K. Highbarger, M. H. Key, R. Kodama, K. Krushelnick, I. Musgrave, H. Nakamura, M. Nakatsutsumi, N. Patel, R. Stephens, M. Storm, M. Tampo, W. Theobald, L. Van Woerkom, R. L. Weber, M. S. Wei, N. C. Woolsey, and P. A. Norreys, *Nat. Phys.* **3**, 853 (2007).
- ⁸H. Hora, *Laser Part. Beams* **27**, 207 (2009).
- ⁹H. Hora, G. H. Miley, M. Ghoranneviss, B. Malekynia, N. Azizi, and X. He, *Energy Environ. Sci.* **3**, 479 (2010).
- ¹⁰A. A. Solodov, K. S. Anderson, R. Betti, V. Gotcheva, J. Myatt, J. A. Delettrez, S. Skupsky, W. Theobald, and C. Stoeckl, *Phys. Plasmas* **16**, 056309 (2009).
- ¹¹V. Malka, J. Faure, Y. A. Gaduel, E. Lefebvre, A. Rousse, and K. T. Phuoc, *Nat. Phys.* **4**, 447 (2008).
- ¹²C. T. Zhou, X. G. Wang, S. C. Ruan, S. Z. Wu, L. Y. Chew, M. Y. Yu, and X. T. He, *Phys. Plasmas* **17**, 083103 (2010).
- ¹³S. C. Wilks and W. L. Kruer, *IEEE J. Quantum Electron.* **33**, 1954 (1997).
- ¹⁴O. Polomarov, I. Kaganovich, and G. Shvets, *Phys. Rev. Lett.* **101**, 175001 (2008).
- ¹⁵H. B. Cai, K. Mima, W. M. Zhou, T. Jozaki, H. Nagatomo, A. Sunahara, and R. J. Mason, *Phys. Rev. Lett.* **102**, 245001 (2009).
- ¹⁶C. T. Zhou, X. T. He, and M. Y. Yu, *Appl. Phys. Lett.* **92**, 151502 (2008); *Appl. Phys. Lett.* **92**, 071502 (2008).
- ¹⁷S. Z. Wu, C. T. Zhou, and S. P. Zhu, *Phys. Plasmas* **17**, 063103 (2010).
- ¹⁸W. H. Bennett, *Phys. Rev.* **98**, 1584 (1955).